Characterization of the tunneling conductance across DNA bases

Radomir Zikic,[1] Predrag S. Krstić,[1] X.-G. Zhang,[2,3] Miguel Fuentes-Cabrera,[2,3] Jack Wells,[2,3] and Xiongce Zhao[3]
[1]*Physics Division, Oak Ridge National Laboratory, P.O. Box 2008, Oak Ridge, Tennessee 37831, USA*
[2]*Computer Science and Mathematics Division, Oak Ridge National Laboratory, P.O. Box 2008, Oak Ridge, Tennessee 37831, USA*
[3]*Center for Nanophase Materials Sciences, Oak Ridge National Laboratory, P.O. Box 2008, Oak Ridge, Tennessee 37831, USA*
(Received 8 February 2006; published 28 July 2006)

Characterization of the electrical properties of the DNA bases (adenine, cytosine, guanine, and thymine), in addition to building the basic knowledge on these fundamental constituents of a DNA, is a crucial step in developing a DNA sequencing technology. We present a first-principles study of the current-voltage characteristics of nucleotidelike molecules of the DNA bases, placed in a 1.5 nm gap formed between gold nanoelectrodes. The quantum transport calculations in the tunneling regime are shown to vary strongly with the electrode-molecule geometry and the choice of the density-functional theory exchange-correlation functionals. Analysis of the results in the zero-bias limit indicates that distinguishable current-voltage characteristics of different DNA bases are dominated by the geometrical conformations of the bases and nanoelectrodes.

DOI: 10.1103/PhysRevE.74.011919 PACS number(s): 87.15.−v, 82.39.Jn, 87.64.Aa

I. INTRODUCTION

There has been significant demand and research activity for the development of new DNA sequencing technologies [1]. The recent achievement in completing the first reference human genome sequence [2] is just the beginning of a revolution that could potentially lead to a genome-based medical practice. For genome-based medical treatment to become a reality, and for medical practitioners to routinely analyze an individual's DNA in a clinical setting, technology is needed that can perform sequencing at a speed thousands of times faster than that of the current technology. For example, recently an interesting approach characterized DNA by measuring changes of ionic conductivity across a membrane that were caused by the threading of a polynucleotide molecule through a channel or nanopore in the membrane [3,4].

Charge transport through biological molecules ultimately depends on the electronic and chemical structure of these molecules, altered by the presence of the electrodes. In this paper, we explore whether the unique conductance signatures of the DNA bases can be used to sequence DNA. The rationale is that the electronic and chemical structure of the four DNA bases [adenine (*A*), cytosine (*C*), guanine (*G*), and thymine (*T*)] are intrinsically different, and should, in principle, produce distinguishable electron transport properties [5]. Assuming that a practical way could be found to thread a single stranded-DNA polymer (ssDNA) through the nm gap formed by two gold (Au) nanoelectrodes, the DNA sequence could be read from conductivity measurements as a function of the position of the polymer in the gap. A fundamental element of such a method is the conductance through the DNA bases.

The electronic transmission of a molecule is critically dependent on the contact between electrode and molecule [6], which largely explains the orders of magnitude disagreement between theory and early, groundbreaking scanning tunnel microscopy (STM) experiments in the molecular electronics [7]. In the case of nucleotides, both sugar and phosphate groups must be considered as well, for they form part of the single-stranded DNA (ssDNA) and should interact with the electrodes. Additionally, other factors that could influence the conductivity measurements [8,9], such as water molecules, electrolytes, or contamination of the electrodes, might completely change the nature of the conductance to a Marcus-like mechanism [10]. In this paper, we concentrate on the basic mechanism—transverse transport of electrons through a nucleotide molecule placed between two electrodes with a gap 1.5 nm in size, leaving all other factors for future studies.

If, in an experiment, the gap between the electrodes is larger than about 2 nm, the charge transport is likely dominated by the diffusion process [11]. Coherent quantum tunneling is important if the electrodes are closer than this distance. In our study, by choosing the nanogap between the electrodes at 1.5 nm, within which we place the DNA-like nucleotides, coherent electron tunneling across the nucleotides is likely the dominant mechanism [12,13] defining the electric transport characteristics of a particular ssDNA in a possible experiment. For each molecule, ten nucleotide-electrode mutual geometries, defined by a rotation around the glycosidic bond (the bond that joins the sugar and the base), hereafter in the text called glycosidic angle, were considered in order to study the effect of geometry on the conductance as well as to represent more reliably an average effect of the different conformations that a ssDNA segment would assume in a possible experiment.

The information on electronic structure of the nucleotides-nanoelectrodes systems to be used in our calculations of the electron transport is obtained from the self-consistent density-functional theory (DFT) calculations using a Gaussian basis. Accurate determination of the parameters relating to the electronic structure, such as the position of the Fermi energy relative to the nucleotide energy levels, is important for obtaining the correct values of the conductance. Such accuracy is also critical in building a correct understanding of the underlying mechanism of the transport process. This consideration motivates us to perform all calculations twice, using different choices of DFT exchange-correlation (XC) functionals, obtaining intermediate and final results that significantly vary, both in absolute and relative values. While our sampling of possible XC functionals is not

exhaustive, we consider the exploration "due diligence" in establishing the acceptability and relevance of our numerical calculations, in the face of the well-known difficulties of the nonequilibrium, quantum many-body problem.

We have read with interest recent reports by Di Ventra and co-workers claiming that the distributions of current values sampled repeatedly for each nucleotide will be sufficiently different to allow for rapid DNA sequencing if some control is exerted on the DNA dynamics [14,15]. The approximations involved in the parametrization intrinsic in the tight-binding model of the Hamiltonian, used in Refs. [14,15], can substantially impact the information on the DNA-nucleotide-electrode electronic structure and its relation to the electrode Fermi energy. This, for example, might influence the conclusion obtained by the authors of Ref. [14] of a strong dominance of the adenine conductance over the *G*, *C*, and *T* nucleotides at low voltage biases (0.1 V). It is not possible to conclude with certainty, as the main information on the electronic structure of the electrode-molecule system, i.e., the alignment of the Fermi level with the electronic structure, is not communicated in Refs. [14,15]. Our analysis, derived from both considerations of the system's electronic structure as computed from DFT, its geometry, and the first-principles conductance calculations at low biases, leads to conclusions that are both qualitatively and quantitatively different from those of Ref. [14], which raises concerns on the agreement of the results of this work with that in Refs. [14,15]. The details of both the system geometry and the DFT calculations that serve as input to our electron transport calculation are described in Sec. II.

Another source of uncertainty could be the inadequacy of the transport theory—1 V of voltage bias between electrodes might be too large for the near-equilibrium—linear-response approximation contained in the Caroli formula that was used in Ref. [15]. We calculate electronic transport properties of the DNA nucleotides between two nanoelectrode tips subject to small electric bias, in the range 0–400 mV. The electron transmission probability, ETP, is proportional to the molecular electronic conductance [16], where the ETP includes the detailed quantum description of the molecule and its interaction with the leads, and is a basic building block in calculation of the *I*-*V* characteristics. The details of the approach are described in Sec. III, while the results of the calculation are presented and discussed in Sec. IV. To construct an understanding on the principal mechanism of the conductance of the DNA nucleotides between two nanowires for low electric bias, we perform in Sec. V a detailed analysis of our results in the limit $V=0$ and for one of the DFT XC functionals. The conductance of various nucleotides and various glycosidic angles are all fitted to a single analytical form appropriate for a combination of the tunneling processes. This result suggests a simple but somewhat unexpected conclusion that the geometry of a base and of the base-electrode ensemble are the dominant critical factors defining reproducible DNA conductance measurements and their mutual distinguishability. Future research in this direction, in particular for finite bias and other variations of geometries, is anticipated. Finally, our conclusions are given in Sec. VI.

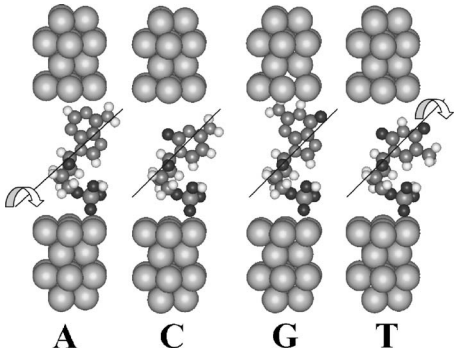

FIG. 1. *A*, *C*, *G*, and *T* bases with sugar-phosphate groups between two gold nanonelectrodes; the sugar-base axis of rotation is indicated in each case, rotation angle here is adopted 0°.

II. THE NUCLEOTIDE-ELECTRODE GEOMETRY AND DENSITY-FUNCTIONAL (DFT) CALCULATIONS

For each molecule, ten nucleotide-electrode mutual geometries, defined by a rotation around the glycosidic bond (the bond that joins the sugar and the base), hereafter in the text called glycosidic angle, were considered. This was done so as to study the effect of geometry on the conductance as well as to represent more reliably an average effect of the different conformations that a ssDNA segment would assume in a possible experiment.

In our models, the following assumptions were made. First, the structures of nucleotides were extracted from B-DNA with a twist angle of 36°. Second, for convenience, and to ensure charge neutrality, two oxygen atoms of the phosphate groups were saturated with H; the carbon 3′ of the sugar group was saturated with H as well. And third, when considering different geometries, only the bases were rotated in terms of the glycosidic angle, which were varied from 0° to 90° in increments of 10°. None of the structures considered in this work were relaxed, unlike the structures considered in Ref. [14]. Figures 1 and 2 show two limiting conformations, for 0° and 90°, respectively, for adenine, cytosine, guanine and thymine (with sugar and phosphate groups) placed in between two Au nanoelectrodes. The electrical response of a lead-molecule-lead system, called thereafter an extended molecule, is strongly dependent on the mutual ge-

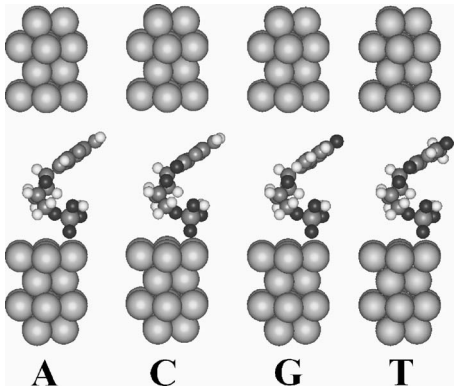

FIG. 2. The nucleotide-nanoelectrode geometries of Fig. 1 for rotations of 90°.

ometry of the leads and the molecule. To account for a variety of possible geometric configurations, we perform the calculation of the *I-V* characteristics for a series of positions obtained by rotation of the bases about the axes indicated in Fig. 1. The gold leads are separated by a fixed distance of 1.5 nm. A layer of a lead contains two sublayers in (111) geometry, of seven and three atoms, as can be seen at Fig. 1, where two layers of each lead are shown. The diameter of the Au interfacial hexagon is close to 6 Å.

For the systems and geometries indicated in Figs. 1 and 2, the Hamiltonian and the overlap matrices were obtained from the converged self-consistent DFT calculations. For description of the nanoelectrodes and their Fermi energy, a separate calculation of the five-layer gold electrode was also performed. The DFT calculation was executed using the computational chemistry package NWCHEM [17]. The semi-infinite lead Green's function was calculated by applying the generalized tight-binding procedure [18,19]. The Gaussian basis based on the CRENBL-effective core potentials (ECP) [17], with 16 (4*s*4*p*) functions for each atom of N, C, O, and P and 4 (4*s*) functions for each H, as well as CRENBS-ECP basis consisting of ten (1*s*1*p*1*d*) functions for each atom was used for Au. This choice of the bases resulted in up to 800 basis functions describing the quantum system. The calculations were executed at 16 processors SGI Altix.

Similar to the results of our earlier work [19], the calculated conductance characteristics of a molecule are sensitive to a choice of the DFT exchange-correlation functional. In absence of the functionals calibrated specifically for the metal-organic system studied, we performed two complete sets of calculations, with the *b3lyp* functional (extensively used for organic molecules), denoted in the rest of text as XC1, and with the *pbe*0 functional (used for Au and other transition metals), denoted by XC2. This resulted in two sets of results, which are compared in the following sections.

At this point, we show two results that emerge directly from the DFT–XC1 calculation. The molecular orbitals of the extended molecule are of particular interest because they may provide clues for the connection between the electronic structure and conductance properties of the nucleotides. A diagram of the extended molecule's eigenenergy levels is presented in Fig. 3. Both the highest occupied molecular orbital (HOMO) and lowest unoccupied molecular orbital (LUMO) in all cases are composed of the gold atomic wave functions, localized in the leads. Although the HOMO states, which are close to the Fermi energy of the leads, provide the electrons for tunneling across the molecular barrier, there are no states localized at the nucleotide in the vicinity of the Fermi energy that can provide a conduction channel through the molecule. Consequently, tunneling through the vacuum gap and across the molecule via the evanescent (decaying) tails of the electronic states in the gold electrodes is more likely to be the driving mechanism of conduction. Of course, this process is highly dependent on the geometrical characteristics of the electron tunneling paths. And as will be discussed more in Sec. V, it is especially sensitive to the size of the base-lead gap, which is the smallest for the guanine base at small glycosidic angles (Fig. 1), leading to the largest conductance in that case.

In Fig. 4 we show the electron density integrated over the cross section of the molecule in the plane perpendicular to

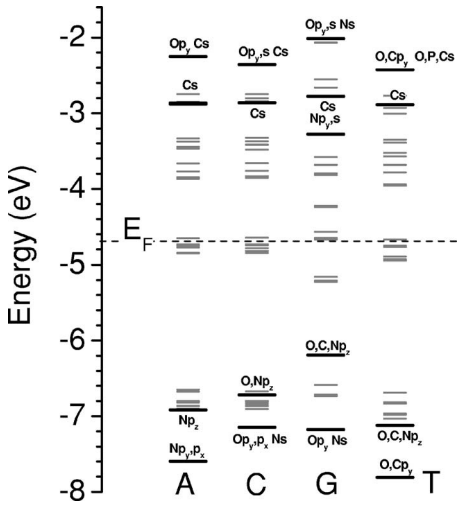

FIG. 3. Molecular eigenenergy levels for the extended molecules with *A*, *G*, *C*, and *T* bases.

the electrodes for the two lowest unoccupied orbitals for the extended molecule of lead-adenine-lead at $\theta=10°$. Both orbitals are localized within the gold electrode at the top, with evanescent tails extending exponentially into the molecule. Several things can be noted from this figure. First, there is clearly a much faster decay in the gap between the top of the molecule and the top electrode (vacuum gap) than within the molecule. Second, while there is no oscillation in the density within the vacuum gap, there are obvious oscillations of the density in the rest of the wave function, indicating that the complex wave vector in this region has a nonzero real part, unlike the vacuum region where the wave vector is purely imaginary. The orbital densities of the extended molecules of other nucleotides near the Fermi energy have similar features. The imaginary parts of the wave vectors for these orbitals are very close, and for the molecule region (excluding the vacuum gap) the imaginary parts of the wave vector averages to about 1.02/Å. This has an important significance in the transport picture, as we will discuss later in the text.

Another direct result of the DFT calculation is the total energy of the cluster of nucleotide+leads, shown in Fig. 5 as functions of the rotation (glycosidic) angle θ. The energy is minimal for small θ ($\theta_{\min}\approx 0$) for extended molecules with

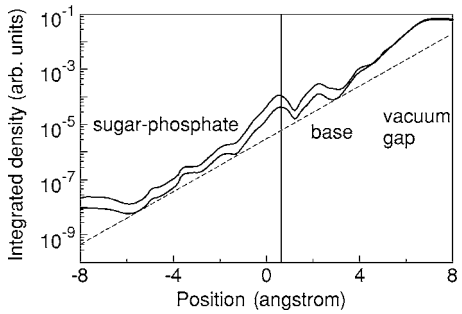

FIG. 4. Electron wave density for two lowest unoccupied orbitals of the extended molecule of lead-adenine-lead at rotation angle of 10°. The straight line is an exponential function with the exponent $\exp(-1.1x)$.

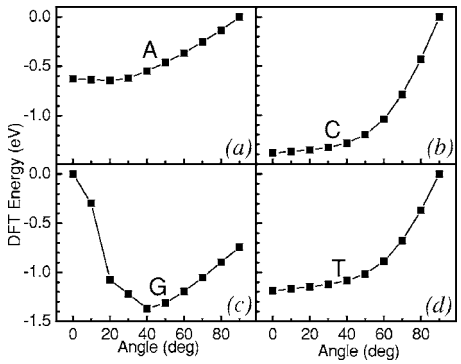

FIG. 5. Total ground state DFT energy of the nucleotide-electrodes cluster, as function of the glycosydic angle. Zeros in figures correspond to −1583.903, −1574.421, −1599.879 and −1586.795 hartrees for *A*, *G*, *C*, and *T* nucleotides (between Au leads), respectively.

all bases except for guanine that minimizes about $\theta_{\min}=40°$. This result indicates that the guanine may take spontaneously larger glycosidic angles than other nucleotides. This is important in a calibration experiment of the DNA sequencing against the nucleotide conductance since the dominance of the *G* conductance that exists at small angles might be that way counterbalanced by the larger $\theta_{\min}$. We perform additional checks of the preferred configurations of the nucleotides in the gap made of gold electrodes by performing a molecular dynamics (MD) simulation of ssDNA molecules translocation through a 2.0 nm nanogap in aqueous environment (details of the MD method can be found in Sec. III). Consistent with the results obtained from the minimum energy principle, the MD calculation also yields qualitatively similar conclusions. Figure 6 shows the probability distribution of the glycosidic angles for four types of single strand nucleotides confined in the Au nanoelectrode gap. For polyA, polyC, and polyT nucleotides, the most probable glycosidic angles peak at about $\theta\approx 0$, but for polyG nucleotide at $\theta\approx 60°$. These preliminary agreements between the MD and quantum mechanical (QM) simulations indicate that geometry factor may play a non-negligible role in the tunneling conductance of nucleotides between nanoelectrodes. However, in consideration of possible complicating factors in a real experimental device, such as applications of electric bias, unbalanced charges (phosphorous group) in the DNA backbone, and electrolyte environments, we are reluctant to

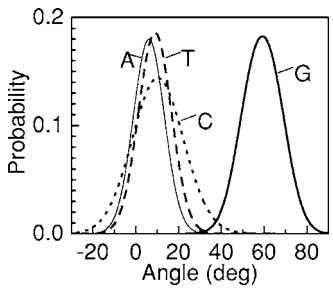

FIG. 6. Glycosydic angle probability distributions obtained from MD modeling for the *A*, *C*, *T*, and *G* nucleotides between two gold electrodes.

take our results as conclusive before more extensive experimental or theoretical studies are performed. Thus, in the following analysis we occasionally apply averaging, not for the purpose of comparing with future experiments, but rather to decrease the number of parameters, while focusing on quantities calculated for various nucleotides. In this reduction procedure, we choose the simplest of all—uniform arithmetic averaging.

III. THEORETICAL METHOD FOR ELECTRON-TRANSPORT CALCULATION

The electron transmission probability, ETP, is proportional to the molecular electronic conductance [16]. We assume nearly thermodynamic equilibrium and a very small voltage drop across the lead-molecule-lead system (from zero to 400 mV), the so-called linear-response regime [20]. Within these assumptions, we describe the electronic structure of the system with density functional theory (DFT) for the ground state in computing the transport properties. This avoids more laborious self-consistent treatment of electronic structure and transport phenomena simultaneously. To describe the open boundary conditions appropriate for the leads, we use the Green's function method in conjunction with the generalized tight-binding (TB) approach [18,19] to compute ETP. In particular, ETP is computed in terms of the well known Caroli's formula [21]

$$\mathrm{ETP} = \mathrm{Tr}[\Gamma_L G_M^+ \Gamma_R G_M^-], \tag{1}$$

where $G_M^{\pm}$ is the advanced (+) or retarded (−) Green's function of the base, and $\Gamma_{(\mathrm{L,R})}$ are the self-energy terms describing the coupling of the left (*L*) and right (*R*) leads with the base molecule. The overlap and Hamiltonian (Fock) matrices obtained from the self-consistent Gaussian DFT calculations of the systems containing a base with several closest lead layers are inputs into the conductance analysis. The DFT calculation is described in Sec. II.

The current *I* through the molecule as a function of the applied voltage *V* is an integral of the electronic transmission probability ETP(E,V). The band energy *E* is associated with the applied voltage bias as

$$I(V) = \frac{e}{h}\int_{E_F-eV/2}^{E_F+eV/2} \mathrm{ETP}(E,V)dE. \tag{2}$$

We ensure that the Fermi energy of the leads, E_F, used in computing the transport coefficients is placed correctly with respect to the band structure of the semi-infinite leads by counting the number of electrons per unit cell within either electrode and requiring that number to equal the number density of electrons below E_F.

The electrode Fermi energy is determined by integrating $\frac{1}{\pi}\,\mathrm{Im}\{\int_{-\infty}^{E_F}\mathrm{Tr}[S(ES-H)^{-1}]\,dE$ and adjusting the E_F until the integration equals the number of electrons per unit cell. Note that the trace is taken over the unit cell of the electrodes but the internal summation in the matrix product can go beyond the unit cell depending on the range of *S*. This yields the Fermi energy of the considered nanowire at about −0.172 hartrees, i.e., close to $E_F=-4.69$ eV.

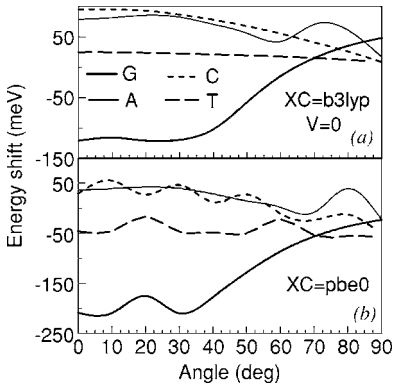

FIG. 7. Potential shifts of the charge neutrality points as functions of the rotation angle from Fig. 1, for two DFT exchange-correlation (XC) functionals.

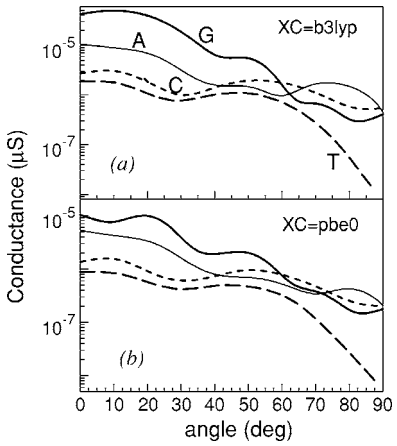

FIG. 8. The conductance of various nucleotides, as functions of angle θ, for the two DFT functionals, (a) XC1=*b3lyp* and (b) XC2=*pbe*0.

Once the electrode Fermi energy is determined, chemical potentials of the left and right electrodes are shifted by $\pm eV/2$ to produce the bias voltage. The neutrality of the electrode-molecule-electrode ensemble provides the addition constraint from which the electrostatic potential of the molecule can be determined for each applied bias voltage. The charge neutrality point of the system is calculated by a contour-integration technique [19], resulting in a voltage-bias dependent shift in the submatrix of the Hamiltonian corresponding to the electrode-nucleotide-electrode molecule, thus extending the "linear response" method beyond a strictly linear one [18]. As far as the self-consistency of the electron transport is considered, this leads to a procedure that is asymptotically exact in limit of zero electric bias, $V \to 0$. The charge neutrality points, expressed in terms of the potential shifts for zero bias are shown at Fig. 7, as functions of the rotation angle θ, for both DFT functionals used, XC1 and XC2.

The obtained potential shifts are of the order of tens of meV, reaching hundreds of meV for the guanine nucleotide. All shifts almost coincide for larger rotational angles θ, reflecting the diminishing coupling of the bases with the electrodes. The shifts are behaving qualitatively similarly for both XC functionals. Since the Fermi energy of the leads and molecular levels of nucleotides are more than 2 eV apart, the potential shifts do not influence the *I-V* characteristics or the calculated conductances (Sec. IV) in any significant way. It is interesting that the potential shifts averaged over angles weakly depend on the applied electric bias up to about $V=0.2$ V, after which these increase slowly and linearly with the bias.

In the MD simulations, the nanogap is composed of two fixed fcc nanoelectrodes (Au, each with dimension of $2\times2\times3$ nm^3). DNA segments of single type nucleotides (polyA, polyC, polyG, or polyT) consists of 20 bases. The DNA, the electrodes and neutralizing counterions (Na+) were solvated in about 21 000 TIP3P [22] water box (initial box size was $11\times7\times9$ nm^3) with three-dimensional (3D) periodic boundary conditions. The DNA and Na+ were modeled by the AMBER force field, 1999 version [22]. The Au atoms in the electrodes were modeled by the universal force field potentials [23]. The Lennard-Jones parameters between different atoms were calculated by the standard Lorentz-Bertholet combining rules. The particle mesh Ewald method was applied to evaluate electrostatic interactions. MD simulations were performed within the constant pressure (1 bar) and temperature (300 K) [24] ensemble. The NAMD [25] software package was employed to integrate the equations of motion. Each simulation included 10 000 steps of energy minimization (conjugate gradient and line search algorithm), 1 ns of molecular dynamics solvent relaxation and equilibration, and 3 ns of production with a time step of 2 fs. The structural configurations were saved every 1 ps for subsequent analysis. Visualizations and analysis were performed using the VMD [26] software packages.

IV. RESULTS

In this section, we review our results for the calculation of the conductance in the zero-bias limit ($V \to 0$), *I-V* characteristics in the range 0–400 mV, and related quantities for all four nucleotides for various angles and DFT functionals. These first-principles results serve as a basis upon which one can build simple models for understanding the conductance properties and mechanisms through the DNA nucleotides. For this purpose, the conductance in the limit $V \to 0$ [proportional to ETP in Eq. (1)] of various nucleotides is shown in Fig. 8, as a function of the glycosidic angle θ. Typical values for conductances are small, varying in range 0.1–1 pS. The XC1 results are about a factor of 3 larger than those for the XC2, showing qualitatively similar though not identical behavior. In the limit of zero bias, the nucleotides are ordered with respect to the magnitude of their conductances as *G*, *A*, *C* and *T*, with approximately a factor of 2 between various bases. The exception is the guanine in the XC1 case, whose conductance is bigger than that of the adenine by almost an order of magnitude. The conductances calculated by the XC1 functional are about a factor of 2 bigger than those by the XC2, except for the guanine, for which the factor reaches about 4.

Figure 9 shows the current, *I*, response for electric biases in the interval 50–300 mV, as functions of glycosidic angle

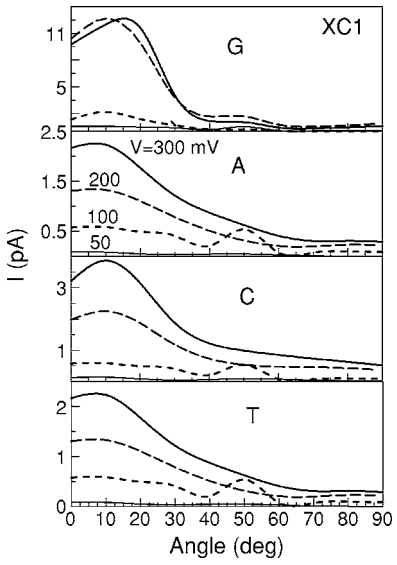

FIG. 9. Angular dependence of the current through various nucleotides, for several voltage biases, calculated with *b3lyp* DFT exchange-correlation functional.

θ. The dominant contribution is for angles up to 40°. In that range, the guanine conductance is obviously dominant. We note that there is a factor of about 2 between XC1 and XC2 currents, similar to the conductances in the limit of $V=0$.

Although the angular dependence of the tunneling current is instructive, it is also of interest how the distinct conductance characteristics displayed in Fig. 9 for different nucleotides survives averaging over angles. In order to show that the dominant features of the *I-V* curves are unaffected by such averaging, in the next few figures we present *I-V* characteristics of various nucleotides, averaged over various geometries (i.e., angles). The averaging reduces the number of parameters, enabling more transparent comparison of the characteristics carried by various nucleotides as well as by the DFT calculation model (XC functionals). Thus, Figs. 10(a) and 10(b) depict the *I-V* curves of different nucleotides for both XC1 and XC2. The cases in Figs. 10(a) and 10(b) are mutually consistent, showing approximately linear characteristics in the range $V<100$ mV and indicating nearly a constant conductance, and the order *G*, *A*, *C*, *T* counted from higher to lower current. Again, this result is very different

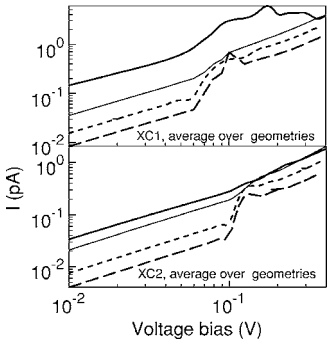

FIG. 10. *I-V* characteristics for various nucleotides and various DFT functionals, averaged over the geometry parameter (θ) of the system; (a) XC1=*b3lyp*; (b) XC2=*pbe*0.

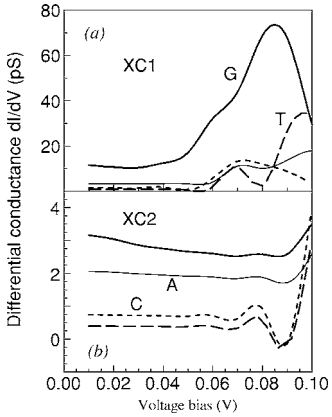

FIG. 11. Angular-averaged differential conductance, dI/dV, as a function of electric bias for various bases and DFT functionals; (a) XC1=*b3lyp*; (b) XC2=*pbe*0.

from that found in Ref. [14], where the ordering is *A*, *G*, *C*, and *T*. In Ref. [15], the ordering is slightly different, i.e., *A*, $G=T,C$, according to their Fig. 3, but *C*, *A*, *T*, *G*, according to their Fig. 1. In our work, XC1 and XC2 gives mutually consistent results, although with XC1 the conductance of the guanine is more dominate than with XC2. In all cases a range of strong nonlinearity around 100 mV brings the curves close to each other, and they stay close at higher biases. Appearance of the nonlinearity in the theory is a consequence of the *V*-dependence in the self-energy terms of the transmission probability in Eq. (2). The first derivatives of the *I-V* characteristics in Fig. 10, the differential conductances, show even more distinctive features, as shown in Fig. 11 for $V<100$ mV, for both functionals. The differential conductance of the guanine with XC1 has a strong peak around 80 mV. The adenine peaked at 65 and 95 mV, while the cytosine has a peak at about 70 mV. Unfortunately the information on the derivatives for XC2 shows quite different and not as distinctive features, Fig. 11(b).

In spite of the apparent transparency of the averaged results in Figs. 12 and 13, having in mind our current, rather arbitrary, choice of a method for averaging, and in absence of arbitraging experiments, any analysis of a physical nature of the obtained results has to relate to a particular geometry of the nucleotide. In order to answer the natural question whether and how are the *I-V* characteristics connected to the

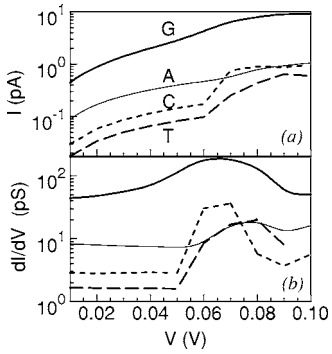

FIG. 12. *I-V* characteristics (a) and differential conductance (b) for $\theta=10°$.

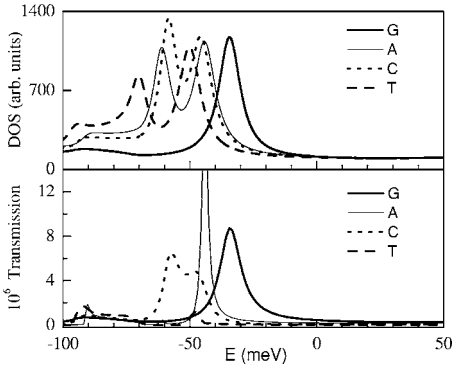

FIG. 13. (a) Density of states (DOS) and (b) transmission probability ETP of the electrodes-molecule system, for various nucleotide, at 10° rotation angle.

electronic structure of the molecule, we examine the *I-V* characteristics of the nucleotides at a particular angle, $\theta=10$, shown at Fig. 12. The linear nature of the characteristics is affected by the form of the transmission functions, which is a function of the applied voltage through the self-energy (Sec. III) and the neutrality point potential shift (Sec. II). Thus, the peaks in the differential conductance reflect the peaks in the transmission function.

The densities of states (DOS) of the systems studied [Fig. 13(a)], shown here for $V=0$ are consistent with the transmission functions, Fig. 13(b), and therefore with the observations above. An applied voltage bias V opens a "conductance window" eV counted from Fermi energy in Fig. 13(b). Consequently, the peaks in the differential conductance in Fig. 12(b) and the peaks in the transmission functions in Fig. 13(b) are in the interval 40–80 mV in the former and 40–80 meV in the latter, somewhat mutually shifted due to the not-shown dependence of the transmission on the applied bias V. Thus, the guanine has the peak closest to the Fermi energy, and it is natural that it dominates the conductance at lower electric biases. Still, this is not an explanation of the mechanism of molecular conductance present here. The density peaks present available channels for conduction in the gold nanowire, the ones that supply the tunneling mechanism explained in the next section where we elucidate our understanding of the electron transport and obtained results in these nonresonant, weakly coupled systems.

V. ANALYSIS OF THE RESULTS IN THE LOW ELECTRIC BIAS LIMIT

In the studies of molecular electronics, one needs to pay close attention to the structure in the *I-V* curves, which reflects the onset of resonances when the Fermi level of the metal electrodes matches the energies of the states in the molecule. From our electronic structure calculation, we see that the states of the extended molecular, i.e., that of the electrode-nucleotide-electrode cluster, near the Fermi energy are all states localized within the electrodes, Fig. 3. Therefore under low electric biases, the conduction electron cannot be resonant with any of the molecular states. Instead, the electron transport characteristics, studied in the previous sections, are most properly described by the tunneling process from the upper to the lower electrode at Figs. 1 and 2 via the nucleotide. As discussed in the previous section, the density-of-states peaks near the electrode Fermi energy correspond to the electron states within the gold lead, and the corresponding peaks in the transmission probability reflect the channels available to tunneling. It is the geometrical conformations of the different nucleotides, their shapes and dimensions in the fixed nanogap that define the various conductance characteristics of the nucleotides with the fixed sugar-phosphate group.

The analysis here is expanded on the work in Ref. [27]. A simple tunneling model is constructed for the limit of $V=0$. We divide the region between the electrodes into three parts that can be recognized in Fig. 1: a vacuum barrier between the top electrode and a DNA base; the base, which is rotated by angle θ around the glycosidic bond; and the sugar-phosphorous group, together with the gap to the bottom electrode, which are fixed and to all bases and is assumed to give a constant factor in the conductance. Each part is approximated as an independent tunnel barrier and contributes a factor to the conductance. The total conductance is then the product of these factors. Next, we find approximations for the factors within each region. The first part can be viewed as a vacuum gap, and thus contributes a simple exponential factor, $\exp(-k_0 d)$, to the conductance, where ik_0 is the imaginary wave vector describing the tunneling through vacuum, and d is the distance from the top electrode to the nearest atom of the molecule. Due to a high sensitivity of the decay exponential on d, this factor proves to be critical for the distinguishability of the various nucleotides by their conductances at Figs. 9 and 10. The second region, the DNA base, yields a factor, $F(\theta)$, that depends on the angle of rotation θ. Combining these two factors and absorbing the constant due to region three into $F(\theta)$, we express the conductance in the form

$$g = F(\theta)e^{-k_0 d}. \tag{3}$$

The precise form for $F(\theta)$ depends on the geometric dimension of the DNA base. The base part of the molecule, i.e., the part that rotates, is modeled by a rectangular box with the dimension $\ell_1 \times \ell_2 \times a$. Along the direction of the electrodes, the linear dimension of the base is ℓ_1. Perpendicular to this direction and the glycosidic bond the linear dimension is ℓ_2. a is the "thickness" of the base. The value of ℓ_1 is measured by the difference in the height of the nucleotide at $\theta=0°$ and at $\theta=90°$. Strictly speaking, this value should be $\ell_1-\ell_2$ from which ℓ_1 can be deduced. However, this difference does not impact our simple model, so we neglect it for the sake of simplicity. The parameter ℓ_1 varies with nucleotides and is fitted from the geometry, while ℓ_2 is assumed to be the same for all nucleotides. In the second region the electron can either tunnel through the vacuum or along the base. Because this region is only a few angstroms in size, we assume that all paths are coherent. The wave function amplitude for tunneling along a path first travels in vacuum for a distance of x along the direction of the electrodes, then travels along the base for a distance of ℓ_1-x, reaching the pivot point between the base and the sugar-phosphate group, is $\exp\{-[k_0 x \cos\theta$

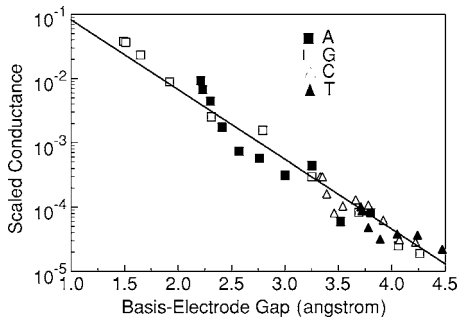

FIG. 14. Normalized conductance, $g/F(\theta)$, as a function of the distance between the top electrode and the nearest atom of a nucleotide, for $V=0$. The solid line is the exponential $\exp(-k_0 d)$ with $k_0=2.5/\text{Å}$. Symbols represent scaled conductance for various angles and nucleotides, obtained by the first-principles calculation of Sec. IV.

$+k_1(\ell_1-x)]/2\}$, where x takes a value between 0 and ℓ_1 and the phase of the wave function is neglected (equivalent to an assumption that the wave vectors are imaginary along all paths, including those inside the molecule). Since the effective cross section for each path is $dxa \sin\theta$, integrating the amplitudes over x, we find

$$F(\theta) = g_0 \left[1 + \frac{2 \sin\theta (e^{(k_1 - k_0 \cos\theta)\ell_1/2} - 1)}{(k_1 - k_0 \cos\theta)\ell_2} \right]^2, \qquad (4)$$

where g_0 is a constant independent of geometric parameters but may be different for each type of nucleotide, and ik_1 is the pure-imaginary wave vector inside the molecule. An overall factor $a\ell_2 \exp(-k_1\ell_1)$ has been absorbed into g_0.

Some of the parameters in Eq. (4) can be determined directly from the geometry. Thus, the values of ℓ_1 are 1.6, 0.89, 2.7, and 0.8 Å for A, C, G, and T nucleotides, respectively. From the first-principles DFT calculation in the previous sections, we already determined that $k_1=1.02/\text{Å}$. The rest of the parameters are fitted from the results for conductance for $V=0$ explained in the previous section, and shown in Fig. 8.

To compare our conductance calculations of previous sections with the simple model given by Eq. (3), we need to examine the θ dependence and the dependence on d separately. In Fig. 14 we plot the normalized conductance, with the θ dependence removed in the form $g/F(\theta)$, as a function of d. The fitted parameters in Eq. (4) are $k_0=2.5/\text{Å}$, $\ell_2=2$ Å, and the values of g_0 are 2.8×10^{-5}, 2.2×10^{-4}, 3.4×10^{-5}, and 4.5×10^{-4}, in units of quantum conductance e^2/h, for A, C, G, and T nucleotides, respectively. For the case of the thymine at $\theta>60°$, the conductance drops sharply to nearly zero and is not plotted on the figure. We also note that the fitted decaying wave vector of $k_0=2.5/\text{Å}$ corresponds to a barrier height of 5.7 eV for an electron effective mass of 1. This is in good agreement with the surface work function of gold around 5.5 eV. The cause of much higher conductance of the guanine than other nucleotides at small angles is clear from this plot. As discussed in Sec. II, it is due to the much smaller gap between the molecule and the electrode, which is the result of the larger size of the guanine.

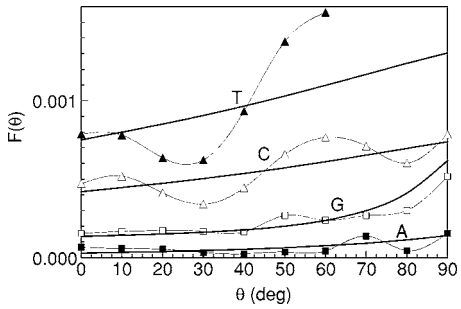

FIG. 15. Angular dependence of the conductance. The data for G, C, and T nucleotides are shifted by 0.0001, 0.0002, and 0.0003, respectively, for visibility. Solid lines are from Eq. (4).

The deviations of our numerical results from the simple exponential are not random. They are oscillations due to quantum interference effect that is neglected in Eq. (4). These oscillations are more clearly seen when we scale out the exponential factor, $\exp(-k_0 d)$, from the conductance and examine the angular dependent factor, $F(\theta)$. In Fig. 15 we plot $F(\theta)$ for all of the nucleotides. Although Eq. (4) captures the trend of the angular dependence pretty well, we see clearly that there are additional large oscillations in the first-principles results. These oscillations arise from the interference effect, neglected during derivation of Eq. (4), between different tunneling paths. If the complex wave vector along any of these paths has a nonzero real part, a summation of the wave function amplitudes over different tunneling paths yields a nonzero phase in the second term of Eq. (4). This can produce an oscillatory cross term in the conductance. A similar effect was predicted in Fe/MgO/Fe tunnel junctions [28]. Such interference effects are often smeared under experimental conditions and may be difficult to observe.

The electronic structure enters Eq. (4) through the decay wave vector k_1 in the molecule, as well as through the overall factor g_0. The former may have a dependence on the HOMO-LUMO gap of the nucleotide. However, k_1 is the same for all molecules and all angles. The prefactor g_0 contains a dependence on the electronic structure of the various nucleotides mainly from the exponential factor $\exp(-k_1\ell_1)$. The vacuum decay factor is determined essentially by the work function of the metal electrode. Neglecting the interference effects, Eq. (3) may serve as a decent model for electron conduction through the DNA nucleotides in the limit $V=0$. A possible extension of this model beyond the linear response regime is not clear and requires further research.

Fitting parameters in Eqs. (3) and (4) were determined from the DFT-XC1 calculations. As shown in Sec. IV use of another exchange-correlation functional yields qualitatively similar, though quantitatively different conductance characteristics of the DNA nucleotides. Therefore, the parameters of tunneling defined in this section serve only to illustrate the mechanism of conductance and may not have meaning beyond such illustration.

VI. CONCLUSIONS

As long as the Fermi level of the electrodes is not resonant with the levels of the molecule, which seems to be the

case with the DNA nucleotide between the gold electrodes, the dominant mechanism of the electric conduction through a gap with a nucleotide is tunneling. Our findings, contained within the calculated conductance characteristics of the nucleotides, indicate a conclusion with an overarching importance for the transverse-conductance measurements of the ssDNA, in particular with respect to the ssDNA sequencing through such measurements. In the absence of a resonance, the geometrical characteristics of the gap and the nucleotide, and the position of the nucleotide relative to the electrodes, are far more important in the determination of the conductance than the parameters usually considered to be significant, such as the values of the HOMO and the LUMO energies. The different nucleotides are thus distinguished in their conductances, largely due to their differences in geometric parameters, such as size, orientation, and bond angles. Future work is required to understand the extent to which this distinguishability survives the refinement of the model systems toward more realistic representations of the ssDNA molecule in an aqueous environment, averaging over the range of possible conformations of ssDNA within the nanoscale channel formed by the leads, and consideration of background Faraday currents, as well as other contributions to observed signal-to-noise ratios. Beyond the geometric considerations, of particular interest would be the study of means to shift the Fermi energy, relative to the energies of the molecular states, while maintaining a low bias between the two nanoelectrodes. Progress in this direction might result in a resonant mechanism of conduction, with orders of magnitude larger conductance than that considered here.

ACKNOWLEDGMENTS

We acknowledge support from National Human Genome Research Institute of the NIH under Grant No. 1 R21 HG003578-01, from the Office of Fusion Sciences (P.K.) and as a user project at the Center for Nanophase Materials Science (CNMS) at ORNL sponsored by the Division of Scientific User Facilities (P,K., X.Z., J.W.), U.S. DOE. We (R.Z., M.F., X.Z.) gratefully acknowledge the support from the ORNL Postdoctoral Research Associates Program administered jointly by Oak Ridge Institute for Science and Education and Oak Ridge National Laboratory. We acknowledge the use of supercomputing resources of the Center of Computational Sciences at ORNL, sponsored by the Office of Science, U.S. DOE. We gratefully acknowledge fruitful discussions with James W. Lee, Thomas Thundat, and Lan Zhang on a number of subjects related to the topic of this paper.

[1] J. R. Shendure, D. Mitra, C. Varma, and G. M. Church, Nat. Rev. Genet. **5**, 335 (2004).
[2] J. C. Venter, M. D. Adams, E. W. Myers *et al.*, Science **291**, 1304 (2001).
[3] J. J. Kasianowicz, E. Brandin, D. Branton, and D. W. Deamer, Proc. Natl. Acad. Sci. U.S.A. **93**, 13770 (1996).
[4] S. Howorka, S. S. Cheley, and H. Bayley, Nat. Biotechnol. **19**, 636 (2001).
[5] J. W. Lee, T. G. Thundat, and E. Greenbaum, U.S. Patent No. 2003141189 A1 (pending).
[6] X. D. Cui, A. Primak, X. Zarate *et al.*, Science **294**, 571 (2001).
[7] M. Di Ventra, S. T. Pantelides, and N. D. Lang, Phys. Rev. Lett. **84**, 979 (2000).
[8] R. G. Enders, D. L. Cox, and R. R. P. Singh, Rev. Mod. Phys. **76**, 195 (2004).
[9] B. Xu, P. Zhang, X. Li, and N. Tao, Nano Lett. **4**, 1105 (2004).
[10] R. N. Barnett, C. L. Cleveland, A. Joy, U. Landman, and G. B. Schuster, Science **294**, 567 (2001).
[11] A. L. Burin and M. A. Ratner, Chem. Phys. **61**, 275 (2002).
[12] D. Porath, A. Bezryadin, S. de Vries, and C. Dekker, Nature **403**, 635 (2000).
[13] J. R. Heath and M. A. Ratner, Phys. Today **56**, 43 (2003).
[14] M. Zwolak and M. Di Ventra, Nano Lett. **5**, 421 (2005).
[15] J. Lagerqvist, M. Zwolak, and M. Di Ventra, Nano Lett. **6**, 779 (2006).
[16] R. Landauer, IBM J. Res. Dev. **1**, 233 (1970); Philos. Mag. **21**, 863 (1957).
[17] D. E. Bernholdt, E. Apra, H. A. Früchtl *et al.*, Int. J. Quantum Chem. **29**, 475 (1995).
[18] P. S. Krstic, X.-G. Zhang, and W. H. Butler, Phys. Rev. B **66**, 205319 (2002).
[19] P. S. Krstic, D. J. Dean, X.-G. Zhang, D. Keffer, Y. S. Leng, P. T. Cummings, and J. C. Wells, Comput. Mater. Sci. **28**, 321 (2003).
[20] C. Joachim, J. K. Gimzewski, and A. Aviram, Nature **408**, 541 (2000).
[21] C. Caroli, R. Combescot, P. Nozières, and D. Saint-James, J. Phys. C **4**, 916 (1971).
[22] W. L. Jorgensen, J. Am. Chem. Soc. **103**, 335 (1981); D. A. Case, *et al.*, AMBER 8 (University of California, San Francisco, 2004)
[23] A. K. Rappé, C. J. Cassewit, K. S. Colwell, W. A. Goddard III, and W. M. Skiff, J. Am. Chem. Soc. **114**, 10024 (1992).
[24] H. J. C. Berendsen, J. P. M. Postma, W. F. van Gunsteren, A. D. Nola, and J. R. Haak, J. Chem. Phys. **81**, 3684 (1984).
[25] L. Kale, R. Skeel, M. Bhandarkar, R. Brunner, A. Gursoy, N. Krawetz, J. Phillips, A. Shinozaki, K. Varadarajan, and K. Schulten, J. Comput. Phys. **151**, 283 (1999).
[26] W. Humphrey, A. Dalke, and K. Schulten, J. Mol. Graphics **14**, 1 (1996).
[27] X.-G. Zhang, P. S. Krstic, R. Zikic, J. C. Wells, and M. Fuentes-Cabrera, Biophys. J. **91**, L04 (2006).
[28] W. H. Butler, X.-G. Zhang, T. C. Schulthess, and J. M. MacLaren, Phys. Rev. B **63**, 054416 (2001).